

Author Manuscript

Title: Propane Dehydrogenation to Propylene and Propylene Adsorption on Ni and Ni-Sn Catalysts

Authors: Jason P. Robbins; Lotanna Ezeonu; Ziyu Tang; Xiaofang Yang; Bruce E. Koel; Simon George Podkolzin

This is the author manuscript accepted for publication. It has not been through the copyediting, typesetting, pagination and proofreading process, which may lead to differences between this version and the Version of Record.

To be cited as: 10.1002/cctc.202101546

Link to VoR: https://doi.org/10.1002/cctc.202101546

Propane Dehydrogenation to Propylene and Propylene Adsorption on Ni and Ni-Sn Catalysts

Jason P. Robbins¹, Lotanna Ezeonu¹, Ziyu Tang¹, Dr. Xiaofang Yang²,

Prof. Bruce E. Koel*², Prof. Simon G. Podkolzin*¹

¹Department of Chemical Engineering and Materials Science, Stevens Institute of Technology, Hoboken, New Jersey 07030, United States

²Department of Chemical and Biological Engineering, Princeton University, Princeton, New Jersey 08544, United States

Corresponding Authors: BEK: bkoel@princeton.edu, SGP: Simon.Podkolzin@Stevens.edu, http://podkolzin.com/

Abstract

Temperature programmed reaction (TPR) measurements with propane over silicasupported Ni, Ni-Sn and Sn catalysts show that the reaction products change significantly from mostly methane, hydrogen and surface carbon over Ni to propylene and hydrogen over Ni-Sn. Propylene formation over Ni-Sn starts at a moderate temperature of 630 K. Since the activity of Sn by itself is low, Sn serves as a promoter for Ni. The promoter effects are attributed to a lower adsorption energy of molecularly adsorbed propylene and suppression of propylidyne formation on Ni-Sn based on temperature programmed desorption (TPD) and infrared reflection absorption spectroscopy (IRAS) measurements as well as density functional theory (DFT) calculations for propylene adsorption on Ni(110) and c(2×2)-Sn/Ni(110) single-crystal surfaces. On Ni, propylene forms a π bonded structure with v(C=C) at 1500 cm⁻¹, which desorbs at 170 K, and a di-σ-bonded structure with v(C=C) at 1416 cm⁻¹, which desorbs at 245 K. The di- σ -bonded structure is asymmetric, with the methylene C being in the middle of the Ni-Ni bridge site, and the methylidyne C atom being above one of these Ni atoms. Therefore, this structure can also be characterized as a hybrid between di- σ - and π -bonded structures. Only a fraction of propylene desorbs from Ni because propylene can convert into propylidyne, which decomposes further. In contrast, propylene forms only a π -bonded structure on Ni-Sn with v(C=C) at 1506 cm⁻¹, which desorbs at 125 K. The low stability of this structure enables propylene to desorb fully, resulting in high reaction selectivity in propane dehydrogenation to propylene over the Ni-Sn catalyst.

1. Introduction

Propylene is used in the production of many high-volume chemicals, such as polypropylene and other polymers, propylene oxide, propionaldehyde, acrolein, acrylonitrile and acetone. Accordingly, the demand for propylene is projected to increase steadily. [1, 2] Propylene has been traditionally produced from a mixture of light olefins — ethylene, propylene and butenes — obtained through steam cracking of naphtha or light diesel or as a side product of fluid catalytic cracking (FCC) of heavier oil fractions. Recently, however, it has become more economical to produce ethylene by steam cracking of ethane derived from shale gas, leading to a decrease in the traditional production of olefin mixtures. This change created an imbalance in the production of light olefins with an abundance of ethylene on one side and a shortage of propylene and butenes on the other. As a result, there is a demand for new technologies that can efficiently produce propylene as the target product.

There are two main commercial technologies for the direct non-oxidative production of propylene from propane ($C_3H_8 = C_3H_6 + H_2$): the Catofin process by CB&I Lummus, which uses a CrO_x/Al_2O_3 catalyst, and the Oleflex process by UOP, which uses a Pt-Sn/Al₂O₃ catalyst. However, both technologies have disadvantages due to catalyst coking and sintering of active metals, Cr and Pt, leading to rapid catalyst deactivation. The need for continuous catalyst regeneration complicates the process and increases energy consumption. In addition, high reaction temperatures of 800-980 K further increase energy consumption. Therefore, there are intensive research efforts directed at developing alternative catalysts. [1-4]

Ni is cheaper than Pt and less hazardous than Cr. Ni catalysts are used commercially for multiple reactions, including water-gas shift, steam reforming and hydrogenation. Although pure Ni catalyzes only methane, hydrogen and coke formation in propane reactions, addition of Au

was shown to be promising as the product distribution for Ni-Au significantly shifted to propylene and C₂ hydrocarbons.^[5] In addition, computational screening of 12 metals and multiple bimetallics identified Ni-Mo as a promising catalyst for propane dehydrogenation to propylene.^[4] Furthermore, Ni-Sn catalysts were shown to be promising in isobutane dehydrogenation to isobutene.^[6]

In this work, temperature programmed reaction (TPR) experiments with silica-supported Ni, Ni-Sn and Sn catalysts demonstrate that Ni-Sn is highly selective in catalyzing propane dehydrogenation to propylene without concurrent production of methane or C₂ hydrocarbons. Moreover, propylene formation starts at a moderate reaction temperature of 630 K. In contrast to suggestions in some publications that Ni acts as a promoter for Sn, our results show the opposite: that Sn serves as a promoter for Ni, similarly to Pt-Sn.

The reasons why the propane reaction products change dramatically from methane and carbon for Ni/SiO₂ to propylene for Ni-Sn/SiO₂ were identified by studying differences in propylene adsorption at the molecular level on Ni and Ni-Sn single-crystal surfaces with temperature programed desorption (TPD), infrared reflection absorption spectroscopy (IRAS) and density functional theory (DFT) calculations. Previous studies for propylene adsorption on Ni with ultraviolet photoelectron spectroscopy (UPS)^[7] and with in situ X-ray photoelectron spectroscopy (XPS)^[8] determined the presence of π - and di- σ -bonded structures. Our results identify their geometries, adsorption energies and vibrational frequencies and how they change on Ni-Sn. An additional previous study determined the formation of a propylidyne structure on Ni with diffuse reflectance infrared spectroscopy (DRIFTS) measurements. ^[9] Our study determines propylidyne properties on Ni and why propylidyne formation on Ni-Sn is suppressed. In contrast with some previous computational studies of propane dehydrogenation on Ni that did

not consider propylidyne formation, our results demonstrate that propylidyne is critical in defining the reaction selectivity.

2. Experimental and Computational Methods

2.1 Propylene TPD and IRAS for Ni(110) and c(2×2)-Sn/Ni(110)

Desorption and vibrational spectra were collected for two surfaces: a pure Ni(110) and a Ni-Sn surface obtained by depositing Sn on Ni(110). The Ni(110) crystal (8 mm square, $\pm 0.5^{\circ}$ orientation) was cleaned by sputtering with 1.5 keV Ar⁺ ions and annealing at 1100 K. To eliminate residual carbon, the surface was annealed at an O₂ pressure of 4×10^{-8} Torr at 1000 K. Hydrogen treatments at 4×10^{-8} Torr at 1000 K were used to eliminate residual oxygen. The surface cleanliness was checked with Auger electron spectroscopy (AES), and the surface order and periodicity were verified with the low-energy electron diffraction (LEED) pattern shown in Figure 1a.

The Ni-Sn surface was prepared by depositing 1.0 ML of Sn on the clean Ni(110) and then annealing it at 800 K in an ultrahigh vacuum (UHV) chamber (2×10^{-10} Torr base pressure). The annealed surface exhibited a c(2×2)-Sn/Ni(110) pattern in LEED measurements (Figure 1b). Our previous study with the same preparation procedure demonstrated that Sn was incorporated only in the top layer of Ni(110), forming a surface alloy with a Ni to Sn atomic ratio of unity. [10]

TPD experiments were performed in a three-level, stainless-steel UHV chamber (2×10⁻¹⁰ Torr base pressure), with the sample in the line of sight of the ionizer of a shielded UTI 100C quadrupole mass spectrometer. The shield nozzle was located 1 mm from the sample. The sample was kept in contact with a liquid nitrogen-cooled Cu block that was resistively heated. The temperature was measured with a Chromel–Alumel thermocouple that was spot-welded

directly to the side of the crystal. The heating rate was 3 K/s. Custom software enabled monitoring of up to eight masses simultaneously. The propylene dose was 2×10^{-9} Torr for 60 s.

The IRAS experiments were performed in a separate UHV chamber using a Bruker Vertex 70 instrument with a grazing incidence of 75° from the surface normal and a liquid nitrogen cooled mercury-cadmium-telluride detector. Spectra were obtained with a resolution of 2 cm⁻¹ by averaging 512 scans over 5 min. All adsorption spectra were taken at 90 K by first dosing propylene at 90 K, annealing to the desired temperature and then cooling back to 90 K.

Propylene (Matheson, ultrahigh purity, 99.9%) was purified with freeze-pump-thaw cycles. For both the TPD and IRAS measurements, propylene was introduced into an UHV chamber via a stainless-steel tube doser connected to a variable precision leak valve. After each measurement, residual surface carbon was removed by first annealing in oxygen and then in vacuum at 1100 K prior to the subsequent experiment.

Surface coverage values, θ , are calculated based on the density of Ni atoms on a Ni(110) surface of 1.15×10^{15} atoms/cm², with $\theta = 1$ monolayer (ML) corresponding to one propylene molecule per Ni surface atom to match the coverage notation of the computational results.

2.2 Propane Dehydrogenation over Ni/SiO₂ and Ni-Sn/SiO₂

2.2a Catalyst Preparation

A 1.5 wt % Ni/SiO₂ catalyst was prepared using an incipient wetness impregnation method. Prior to the Ni deposition, the SiO₂ support (Cabot CAB-O-SIL HS-5 fumed silica) was dried by raising the temperature at 1 K/min to 323 K and holding at this temperature for 2 h. After drying, the SiO₂ support was calcined by raising the temperature at 5 K/min to 723 K and holding at this temperature for 2 h. After the Ni deposition (Ni(NO₃)₂·6H₂O, Sigma-Aldrich,

99.999% trace metals basis), the sample was initially dried by first raising the temperature at 1 K/min to 323 K and holding for 4 h and then to 393 K and holding for 2 h. Afterwards, it was calcined by raising the temperature at 5 K/min to 723 K and holding for 2 h. The Ni dispersion was 26% based on H₂ TPD measurements. This measurement agrees with the transmission electron microscopy (TEM) images that showed Ni particles with an average size of 20 nm. A representative TEM image is shown in Figure 2a.

The prepared 1.5 wt % Ni/SiO₂ was split into two samples. The first sample was tested as is, and the second sample was used to prepare a Ni-Sn catalyst by adding Sn (SnCl₂, Sigma-Aldrich, 99.99% trace metals basis) using the same incipient wetness impregnation method and calcined using the same procedure. The Sn to Ni atomic ratio was 0.26, corresponding to the Sn loading of 0.8 wt %. Since Sn was added to Ni/SiO₂, it is likely that most Sn atoms were on the Ni surface with the corresponding surface atomic ratio of 1 to 1, matching the composition of the c(2×2)-Sn/Ni(110) single-crystal surface used in the propylene TPD and IRAS measurements. The addition of Sn did not measurably affect the Ni dispersion. The average size of the metal particles in Ni-Sn/SiO₂ remained about 20 nm (Figure 2b), the same as in Ni/SiO₂ within the experimental accuracy (Figure 2a).

A Sn/SiO_2 catalyst was prepared using the same procedure and the same Sn loading of 0.8 wt % as the $Ni-Sn/SiO_2$ catalyst.

2.2b Catalyst Characterization with H₂ TPD

The metal dispersion of the 1.5 wt % Ni/SiO₂ catalyst was evaluated with H₂ TPD using a Micromeritics AutoChem HP 2950 reactor flow system. A 0.15 g sample was loaded into a U-shaped quartz reactor and secured with quartz wool (Altamira Instruments, Inc.). The system

with the sample was first purged with an Ar (Praxair, ultrahigh purity 99.999%) 50 sccm flow for 30 min. The gas flow was then switched to 20% H₂ (Praxair, ultrahigh purity 99.999%) in Ar with the same total flow rate. The temperature was increased with a rate of 1 K/min to 383 K and held at this temperature for 1 h for drying. The temperature was then increased with a rate of 5 K/min to 723 K and held at this temperature for 2 h for reduction. The temperature was lowered to 303 K in the same flow of 20% H₂ in Ar for H₂ adsorption. Afterwards, the flow of H₂ was stopped, and a 50 sccm Ar flow was used for at least 30 min to remove physisorbed H₂, purge the system and obtain a stable thermal conductivity detector (TCD) baseline for 10 min. TPD was performed by increasing the temperature at 10 K/min to 573 K when all H₂ desorbed. The Ni dispersion of 26% was calculated using the integral area of the TCD H₂ desorption peak, assuming the adsorbed H to surface Ni atomic ratio of unity.

2.2c Reaction Testing

The Ni/SiO₂, Ni-Sn/SiO₂ and Sn/SiO₂ catalysts as well as the SiO₂ support were tested for propane dehydrogenation to propylene in the same Micromeritics AutoChem HP 2950 reactor flow system, which was used for the H₂ TPD measurements. However, instead of the TCD, the reaction products were analyzed with a Hiden Analytical HPR 20 mass spectrometer (MS) by monitoring the following masse-to-charge ratios: 2 (H₂), 16 (CH₄), 26 (C₂H₄), 30 (C₂H₆), 42 (C₃H₆) and 44 (C₃H₈). The expected contribution of propane to the propylene parent mass of 42 was subtracted. Prior to testing, the catalyst was dried and reduced in situ using the same procedure as during the TPD measurements. After the reduction, the temperature was lowered to 333 K in a 50 sccm Ar flow and held at this temperature for 1 h. The flow was then switched to 50 sccm 20% C₃H₈ (Praxair, PR 2.5IS-KN, 99.5 wt %) in Ar at 333 K for 30 min to

ensure a stable MS baseline. The catalysts were tested with temperature programmed reaction by increasing the temperature at 10 K/min to 973 K.

2.3 Computational Methods

Gradient-corrected periodic DFT calculations with the DMol³ code^[11, 12] in Materials Studio 2017 by BIOVIA Corporation were performed for determining geometries, adsorption energies and vibrational frequencies for propylene on Ni(110) and c(2×2)-Sn/Ni(110) surfaces, the same two single-crystal surfaces that were used in the experimental TPD and IRAS measurements. Molecularly and dissociatively adsorbed propylene structures were evaluated on multiple sites for each surface. The calculations used the double numerical with polarization (DNP) basis set and the generalized gradient-corrected Perdew-Wang (GGA PW-91) functional. Tightly bound core electrons were represented with semicore pseudopotentials. Reciprocal-space integration over the Brillouin zone was approximated through k-point sampling with a separation of 0.4 nm⁻¹ using the Monkhorst-Pack grid: 4×5×1. A value of 0.08 for both charge and spin density mixing with direct inversion in the iterative subspace (DIIS) and orbital occupancy with thermal smearing of 0.002 Ha were used. The orbital cutoff distance of 0.4 nm was set for all atoms.

An infinite Ni(110) surface was constructed using a $2\times2\times5$ periodic unit cell shown in Figure 3a. A top view of the two top layers is also shown in Figure 1a. The unit cell had 2×2 surface Ni atoms and 5 layers for a total of 20 Ni atoms. The unit cell was generated from the bulk crystal using the optimized Ni lattice constant of 0.3541 nm, within 0.5% of the 0.3524 nm experimental value. A vacuum spacing of 3 nm in the c direction was used. The $c(2\times2)$ -Sn/Ni(110) surface was constructed by substituting half of the surface Ni atoms in the Ni(110) unit cell with Sn, as shown in Figure 3b. A top view of the two top layers is also shown in Figure

1b. The top three layers of the unit cells were relaxed and optimized with adsorbates during geometry optimizations, accounting for surface relaxation after adsorption. The remaining two bottom layers were constrained at the bulk Ni positions, accounting for the bulk structure. Similarly constructed periodic surfaces with similar computational settings were previously used successfully for studying adsorption and reactions on Ni^[13] and other metal surfaces.^[14-23]

Adsorption energies were calculated at 0 K without zero-point energy corrections using as a reference the sum of energies for the corresponding clean surface and an isolated propylene molecule calculated separately. Adsorption energies are reported as positive numbers, $-\Delta E_{ads}$. Frequency calculations were performed using a partial Hessian matrix for the adsorbed hydrocarbon structures. All vibrational frequencies are reported as calculated, without any adjustments.

3. Results

3.1 Propane Dehydrogenation to Propylene

The reactor testing results for the 1.5 wt % Ni/SiO₂ catalysts with and without Sn (0.8 wt % Sn, 1:1 atomic ratio of Ni to Sn on the surface) are compared in Figure 4. In addition, the results of a blank experiment for the SiO₂ support are included in this figure for comparison. Propane starts reacting on Ni at 475 K. A decline in the propane concentration is observed at this temperature in Figure 4a (mass 44) with simultaneous evolution of hydrogen in Figure 4c (mass 2). Since no concurrent propylene production is observed in Figure 4b (mass 42), propane must be mostly dehydrogenating to produce a carbonaceous residue on the catalyst surface. Propane starts reacting on Ni-Sn at a higher temperature of 630 K. However, in contrast with the Ni catalyst, hydrogen evolution is accompanied by propylene production. While only a trace amount

of propylene is produced on Ni at 610 K, Ni-Sn is highly selective for propane dehydrogenation to propylene (Figure 4b). Furthermore, the presence of Sn suppresses C-C bond breaking reactions. For Ni, methane (mass 16) evolution becomes significant at 685 K (Figure 4d). In contrast, no methane is observed on Ni-Sn up to 800 K. Above this temperature, the onset of methane production on Ni-Sn coincides with that on SiO₂.

The results for the 0.8 wt % Sn/SiO₂ catalyst are close to those for the blank SiO₂ support and, therefore, not shown in Figure 4. Only trace amounts of propylene and hydrogen are detected for Sn starting at ~740 K.

In summary, the addition of Sn decreases the reactivity of propane on Ni but significantly increases the desirable dehydrogenation to propylene and eliminates undesirable cracking to methane. A comparison with the results for the SiO₂ support in Figure 4 demonstrates that these are catalytic effects due to the presence of Sn on the Ni surface because propane reacts in the presence of SiO₂ due to thermal decomposition only at temperatures above 800 K and since Sn by itself in the same concentration as in the Ni-Sn catalyst has a very low activity.

3.2 Propylene TPD

The TPD results for the Ni(110) and c(2×2)-Sn/Ni(110) surfaces are compared in Figure 5. The first propylene desorption peak is observed at ~100 K for both Ni and Ni-Sn (Figure 5a). In contrast, the second propylene desorption peak is observed at 125 K for Ni-Sn, but at a higher temperature of 170 K for Ni. In addition, the second desorption peak is large and sharp for Ni-Sn, as opposed to a small broad feature for Ni with a tail extending to 265 K.

Furthermore, while a large H₂ desorption peak is observed for Ni, no H₂ peak is detected for Ni-Sn in Figure 5b. The H₂ desorption peak for Ni has three features: a shoulder at 265 K, the main peak at a higher temperature of 310 K and a broad tail up to 570 K.

3.3 Propylene IRAS

The IRAS spectra for propylene on the Ni(110) and c(2×2)-Sn/Ni(110) surfaces at 95 K in Figure 6 are similar, with peaks in four regions: 900-1200, 1200-1500, 1500-1700 and 2800-3100 cm⁻¹. The peaks assigned to physisorbed propylene on both surfaces are listed in Table 1. Fewer peaks are observed at 120 K. These peaks are assigned to chemisorbed propylene, and they are summarized in Table 2 for Ni and Table 3 for Ni-Sn. Some peaks for the chemisorbed structures are also observed at 95 K. At higher temperatures, progressively fewer peaks are observed on Ni. There are peaks at 812, 847, 895, 1022, 1207, 2840, 2897 and 2998 cm⁻¹ at 230 K and at 812, 847, 895 and 1360 cm⁻¹ at 480 K. In contrast, no peaks are observed at 240 and 450 K for Ni-Sn.

Additional peaks at 1786, 1799 and 1822 cm⁻¹ at 95, 120 and 230 K, respectively, observed only on Ni are likely due to adsorption of adventitious CO on bridge or threefold Ni sites.^[13, 24, 25]

Table 1. Propylene Vibrational Frequencies, cm⁻¹

vibrational mode	gas phase [26]	calculated isolated molecule	multilayer on Ni and Ni-Sn at 95 K, Figure 6
ω(CH ₂)	912	919	910
ν(C-C)	919	921	910
ρ(CH ₃)	935	927	933
τ(CH ₂)	990	1019	990
ρ(CH ₃)	1045	1047	1041
ρ(CH ₂)	1170	1166	1172
δ(СН)	1298	1295	1295
$\delta_s(CH_3)$	1378	1371	1373
$\delta_s(CH_2)$	1414*	1410	not observed
$\delta_a(CH_3)$	1443	1445	1436
$\delta_a(CH_3)$	1459	1459	1452
ν(C=C)	1653	1667	1647
ν _s (CH ₃)	2932	2954	2840-2890
ν _a (CH ₃)	2953	3003	2929-2941
ν _a (CH ₃)	2973	3040	2964
v _s (CH ₂)	2991	3059	2980
ν(CH)	2991	3070	3067
v _a (CH ₂)	3091	3151	3080

v: stretch, δ: deformation, ρ: rock, τ: twist, ω: wag, s: symmetric, a: asymmetric.

^{*}not observed in gas, only in liquid.

Table 2. Vibrational Frequencies for Molecularly Adsorbed Propylene on Ni, cm⁻¹

	observed	calculated	calculated
vibrational mode	at 120 K, Figure	hybrid di- σ/π -bonded,	π -bonded,
	6a	Figure 7a	Figure 7c
τ(CH ₂)	833	815	832
ω(CH ₂)	868	862	839
ν(C-C)	906	906	897
ρ(CH ₃)	not observed	933	927
ρ(CH ₃)	1022	1023	1017
ρ(CH ₂)	1172	1150	1157
δ(CH)	1207	1199	1242
$\delta_s(CH_3)$	1373	1361	1355
$\delta_s(CH_2)$	not observed	1333	1384
$\delta_a(CH_3)$	not observed	1433	1418
ν(C=C)*	1416	1410	_
$\delta_a(CH_3)$	1452	1451	1446
ν(C=C)	1500	_	1504
v _s (CH ₃)	2840, 2883	2920	2922
v _a (CH ₃)	2998	2973	2980
$\nu_a(CH_3)$	not observed	3019	3008
$\nu_{s}(CH_{2})$	not observed	2844	3030

^{*}C=C double bond becomes a single bond in the di-σ structure.

Table 3. Vibrational Frequencies for Molecularly Adsorbed Propylene on Ni-Sn, cm⁻¹

	observed	calculated π-bonded, Figure 8b	
vibrational mode	at 120 K,		
	Figure 6b		
ω(CH ₂)	not observed	854	
τ(CH ₂)	864	874	
v(C-C)	901	896	
ρ(CH ₃)	916	927	
ρ(CH ₃)	1030	1013	
ρ(CH ₂)	1172	1154	
δ(СН)	1246	1229	
$\delta_s(CH_3)$	1360	1350	
δ_{s} (CH ₂)	not observed	1380	
$\delta_a(CH_3)$	1429	1423	
δ _a (CH ₃)	1452	1445	
ν(C=C)	1506	1507	
v _s (CH ₃)	2840, 2901	2940	
ν _a (CH ₃)	2929	2999	
ν _a (CH ₃)	not observed	3037	
$\nu_s(CH_2)$	not observed	3035	

3.3 DFT Calculations

The calculations show that on substituting surface Ni atoms with Sn atoms, the geometry of the Ni(110) surface changes. The $c(2\times2)$ -Sn/Ni(110) surface is corrugated in contrast with the flat surface of Ni(110) (Figure 3). The surface Ni atoms are in troughs, and the Sn atoms are in ridges, elevated by 0.054 nm. This calculated buckling distance is in line with the experimental estimate of 0.044 \pm 0.005 nm.^[10]

For interpreting the IR spectra of propylene on Ni and Ni-Sn at 95 K, the normal vibrational modes of an isolated propylene molecule were calculated. The calculated vibrational modes were analyzed by visualization and classified as stretch, deformation, rock, twist or wag vibrations. The experimental IR peaks and the corresponding calculated vibrational frequencies are summarized in Table 1. For comparison, Table 1 also includes IR peaks for gas-phase propylene. [26] We note that the peak assignments in Table 1 as well as in Tables 2-4 are based on our analysis of the calculated normal vibrational modes.

Multiple surface sites were evaluated for both molecularly adsorbed propylene and for dissociatively adsorbed propylene as propylidyne (C-CH₂-CH₃) plus hydrogen. The molecular structures are shown in Figures 7 and 8, and their vibrational frequencies are reported in Tables 2 and 3. The bonding of the reported structures with the surface is described with the μ - η notation where the μ index denotes the number of surface metal atoms bonded to the adsorbed hydrocarbon, and the η index denotes the number of carbon atoms in the adsorbed hydrocarbon that are bonded to these metal atoms. On Ni, molecular propylene preferentially adsorbs on a bridge site in a $\mu_2\eta^2$ configuration with an adsorption energy of 112 kJ/mol. In this configuration, the methylene C atom binds to both Ni atoms of the bridge site, and the methylidyne C atom binds only to one Ni atom of the bridge site (Figure 7a). This is an asymmetric di-σ-bonded structure, with the methylene C being in the middle of the Ni-Ni bridge site, and the methylidyne C atom being almost above one of these Ni atoms. This structure can also be described as a hybrid between di- σ - and π -bonded structures because it binds through two C atoms to two metal atoms as a di-σ-bonded structure but also binds through the same two C atoms to a single metal atom as a π -bonded structure. This hybrid between di- σ - and π -bonded structures on a bridge surface site is different than regular di- σ/π -bonded hydrocarbon structures in the $\mu_3\eta^2$

configuration on a threefold metal site, for example, acetylene (CH-CH) or vinylidene (C-CH₂). The hybrid di- σ/π -bonded structure has a bond distance between the bonding C atoms of 0.143 nm, significantly larger than the 0.134-nm C=C double bond in gas-phase propylene. The calculated frequency for the C=C bond stretch, v(C=C), consequently, decreases from 1667 cm⁻¹ for gas-phase propylene (Table 1) to 1410 cm⁻¹ (Table 2). Molecular propylene on the same Ni-Ni bridge site as a regular di- σ -bonded structure is less stable by 17 kJ/mol (Figure 7b), and on a small perturbation, it transforms into the more stable hybrid di- σ/π -bonded structure (Figure 7a). On an atop Ni site, propylene adsorbs as a π -bonded structure (μ I η ² configuration) with an adsorption energy of 90 kJ/mol (Figure 7c), lower than those for a bridge site. Accordingly, the C-C bond distance and v(C=C) for the π -bonded structure of 0.140 nm and 1504 cm⁻¹ are closer to the gas-phase propylene values.

On Ni-Sn, the replacement of half of the surface Ni atoms with Sn isolates each Ni atom in the first layer, eliminating both short and long Ni-Ni bridge surface sites. Since propylene preferentially adsorbs on Ni, not on Sn, there are only two additional potential Ni-Ni bridge sites. On the first additional type, comprising one Ni atom in the first layer and another Ni atom in the second layer, di- σ -bonded structures are calculated to be unstable. On the second additional type, comprising two non-neighboring surface Ni atoms in a diagonal arrangement, di- σ -bonded propylene ($\mu 2\eta^2$ configuration) is calculated to be metastable (Figure 8a). It is higher in energy than gas-phase propylene by 89 kJ/mol and, therefore, such a structure is not likely to form. Thus, the calculations demonstrate that the presence of Sn suppresses the formation of di- σ -bonded propylene.

The only possible remaining adsorption site is a single Ni atom. The π -bonded molecular propylene ($\mu_1\eta^2$ configuration) on an atop Ni site has a calculated adsorption energy of only 21

kJ/mol (Figure 8b), but it is stable. Propylene, therefore, is predicted to be significantly less strongly adsorbed on Ni-Sn than on Ni. The geometry of the π -bonded structure, however, is calculated to change only slightly on Ni-Sn. Consequently, $\nu(C=C)$ increases only slightly by 3 cm⁻¹.

For comparison with the IRAS spectra, the calculated vibrational frequencies in Tables 2 and 3 are listed only for the stable molecularly adsorbed propylene structures, which are expected to be observed experimentally. Frequencies for the di- σ -bonded structures in Figures 7b and 8a are not included because of their instability. Two additional molecular propylene structures on Ni, the $\mu 4\eta^2$ configuration on a fourfold site and the $\mu 2\eta^2$ configuration on a long bridge site (Figure 9) with adsorption energies of 73 and 57 kJ/mol, respectively, are less stable than the structures on short bridge and atop sites (Figure 7a-c). Accordingly, these structures are also not expected to be observed experimentally, and their frequencies are not listed.

When propylene adsorbs dissociatively, it forms propylidyne by splitting off one H atom from the CH₂ group and transferring the remaining H atom to the CH group, similarly to ethylidyne formation from ethylene. ^[28-31] On Ni, propylidyne preferentially adsorbs with an adsorption energy of 99 kJ/mol on a long bridge site by binding to two additional Ni atoms in the second layer in a $\mu 4\eta^1$ configuration (Figure 10a). Propylidyne can also adsorb in a threefold site in a $\mu 3\eta^1$ configuration with a slightly lower adsorption energy of 97 kJ/mol (Figure 10b). Of the three bonding Ni atoms, two are in the first layer, and the third is in the second layer. The split-off H atom preferentially adsorbs in a similar threefold site.

The absence of neighboring surface Ni atoms on Ni-Sn restricts the adsorption of propylidyne to a threefold site formed by one Ni atom in the first layer and two Ni atoms in the

second layer (Figure 10c). The split-off H atom preferentially adsorbs in a similar threefold site. The calculated vibrational frequencies for propylidyne on Ni and Ni-Sn are listed in Table 4.

Table 4. Calculated Vibrational Frequencies for Propylidyne Structures in Figure 10, cm⁻¹

	Ni surface,	Ni surface,	Ni-Sn surface,
vibrational mode	Ni long bridge site,	Ni threefold site,	Ni threefold site,
	Figure 10a	Figure 10b	Figure 10c
$\rho(\mathrm{CH_2})$	749	756	752
ν(C-C)	879	918	860
ρ(CH ₃)	1011	1019	1027
ρ(CH ₃)	1041	1036	1034
ν(C-C)	1023	1085	1017
τ(CH ₂)	1223	1228	1234
ω(CH ₂)	1265	1270	1270
$\delta_s(CH_3)$	1349	1356	1354
δ_s (CH ₂)	1405	1407	1426
$\delta_a(CH_3)$	1420	1428	1430
$\delta_a(CH_3)$	1440	1447	1441
$\nu_s(CH_2)$	2847	2880	2904
v _s (CH ₃)	2908	2904	2932
$\nu_a(CH_2)$	2943	2946	2948
$\nu_a(CH_3)$	2974	3003	2999
$\nu_a(CH_3)$	3017	3049	3021

Although the structure of propylidyne on the threefold site on Ni-Sn (Figure 10c) is similar to that on Ni (Figure 10b), the stability of propylidyne on Ni-Sn is dramatically lower. It is predicted to be metastable (higher in energy) by 146 kJ/mol relative to gas-phase propylene. The calculations, therefore, indicate that the presence of Sn on Ni completely suppresses dissociative propylene adsorption by making propylidyne formation highly energetically unfavorable.

4. Discussion

The first peak at ~100 K in the propylene TPD results in Figure 5a for both Ni and Ni-Sn is due to the desorption of propylene physisorbed as a multilayer. This is evidenced by the low desorption temperature and by the similarities of the propylene IR spectra at 95 K in Figure 6 for both Ni and Ni-Sn to the experimental spectrum of gas-phase propylene and the calculated spectrum of an isolated propylene molecule in Table 1. The IR peak at 910 cm⁻¹ is due to two vibrations with close wavenumbers: the CH₂ wag, ω (CH₂), and the stretch of the C-C single bond, ν (C-C). The peaks in the 930-1200 cm⁻¹ region, namely 933, 990, 1041 and 1172 cm⁻¹, are due to rock and twist vibrations of CH₂ and CH₃: ρ (CH₃), τ (CH₂) and ρ (CH₂). The peaks in the 1200-1500 region, namely 1295, 1373, 1436 and 1452 cm⁻¹, are due to CH, CH₂ and CH₃ deformations: δ (CH), δ (CH₂) and δ (CH₃). The peak at 1647 cm⁻¹ is due to the stretch of the C=C double bond, ν (C=C). And finally, the peaks in the 2800-3100 cm⁻¹ region, namely 2840-2890, 2929-2941, 2964, 2980, 3067 and 3080 cm⁻¹, are due to C-H stretches: ν (CH), ν (CH₂) and ν (CH₃). The desorption temperature of ~100 K for the propylene multilayer for our Ni(110) and c(2×2)-Sn/Ni(110) surfaces is in agreement with that of 105 K reported for Ni(100). [8]

After the desorption of the physisorbed multilayer, a small desorption peak for molecularly chemisorbed propylene at 170 K with a shoulder at 245 K is observed for Ni in Figure 5a. These temperatures are in line with the two TPD peaks at 155 and 225 K reported for Ni(100).^[7] The peak at 170 K can be assigned to the desorption of the π -bonded structure on an atop Ni site in Figure 7c at high surface coverage. With decreasing surface coverage, propylene can occupy a greater number of bridge Ni sites and form the more stable hybrid di- σ/π -bonded structure in Figure 7a, which desorbs at a higher temperature of 245 K. A transition from π - to di- σ -bonded structures was detected for Ni(100) at 150 K with UPS measurements^[7] and

gradually at 105-150 K with in situ XPS measurements. [8] In our IRAS measurements, a mixture of both π -bonded propylene with v(C=C) at 1500 cm⁻¹ and hybrid di- σ/π -bonded propylene with v(C=C) at 1416 cm⁻¹ is observed at 95 and 120 K in Figure 6a. The peak at 1500 cm⁻¹ is not well resolved at 120 K. However, we note that the peak at 1416 cm⁻¹ at this temperature is also small. The calculated v(C=C) values of 1410 and 1504 cm⁻¹ for the hybrid di- σ/π - and π -bonded structures, respectively, in Table 2 agree with the experimental values. Although the CH₂=CH double bond becomes a single bond in the hybrid di- σ/π -bonded structure, its stretch vibration is still labeled as v(C=C) to distinguish it from v(C-C) for the CH-CH₃ bond. The other calculated vibrational frequencies in Table 2 that do not change significantly between the hybrid di- σ/π - and π -bonded structures are also in line with the IRAS peaks at 120 K.

In contrast with Ni, a large single desorption peak at a lower temperature of 125 K is observed for Ni-Sn in Figure 5a, which must be due to desorption of the π -bonded structure on an atop Ni site in Figure 8b. Only π -bonded propylene with $\nu(C=C)$ at 1506 cm⁻¹ is observed in the IRAS measurements at 95 and 120 K in Figure 6a. The lower desorption temperature and the shift of the stretching vibration to a higher wavenumber demonstrate that propylene adsorbs less strongly on Ni-Sn. The DFT results in Figure 8 show that the lower stability of molecular propylene on Ni-Sn is due to both geometric and electronic effects. First, due to the geometric effect, the presence of Sn eliminates Ni-Ni bridge surface sites, which are preferential for propylene adsorption on pure Ni. In addition, di- σ -bonded structures on a bridge site with one Ni atom in the second layer are unstable, and another di- σ -bonded structure on a diagonal Ni-Ni surface site is energetically unfavorable (Figure 8a). As a result, the formation of a di- σ -bonded structure is not possible even at low surface coverage on Ni-Sn, explaining the absence of the desorption peak shoulder at ~245 K and the absence of $\nu(C=C)$ at 1416 cm⁻¹. Second, due to the

electronic effect, the presence of neighboring Sn atoms destabilizes propylene adsorption on Ni. As a result, the same π -bonded structure on an atop Ni site is less stable on Ni-Sn (Figure 8b) than on Ni (Figure 7c), shifting the propylene desorption peak to a lower temperature, from 170 to 125 K in Figure 5a, and shifting ν (C=C) to a higher wavenumber, from 1500 to 1506 cm⁻¹ in Figure 6. This result is consistent with a lower adsorption energy reported for isobutene on Ni-Sn compared to that on Ni.^[32]

The electronic effect is calculated to be more significant than the geometric effect in destabilizing molecularly adsorbed propylene. While the difference in adsorption energies between the π -bonded structures on Ni and Ni-Sn is 69 kJ/mol (electronic effect), the difference in stability between the π - and hybrid di- σ/π -bonded structures on Ni is only 22 kJ/mol (geometric effect). This trend is calculated to be even more pronounced for dissociative propylene adsorption as propylidyne (Figure 10). While the difference in stability between the similar $\mu_3\eta^1$ structures on Ni and Ni-Sn is 241 kJ/mol (electronic effect), the difference in stability for propylidyne on different Ni sites, $\mu_3\eta^1$ and $\mu_3\eta^1$ structures, is only 2 kJ/mol (geometric effect). We note that the geometric and electronic effects cannot be fully separated because the presence of Sn also changes the surface geometry due to corrugation and strain effects.

The significantly smaller size of the propylene desorption peak at 170 K for Ni than that at 125 K for Ni-Sn in Figure 5a indicates that only a small fraction of the chemisorbed propylene desorbs molecularly from Ni. This fraction was previously estimated to be 20% of the saturation coverage based on TPD results for Ni(100).^[7] Most of the chemisorbed propylene decomposes, which is evidenced by the evolution of H₂. The three features of the H₂ desorption peak for Ni in Figure 5b — (1) a shoulder at 265 K, (2) the main peak at 310 K and (3) a broad tail up to 570 K

— are due to progressive decomposition of hydrocarbon surface structures. The first feature at 265 K is consistent with the evolution temperature after H₂ adsorption on clean Ni(110)^[33] and also with that after dissociative acetic acid adsorption on Ni(110). Therefore, the H₂ evolution at 265 K after propylene adsorption on Ni in Figure 5b is limited by H₂ desorption, and not by propylene decomposition. Thus, propylene dehydrogenation on Ni starts at temperatures below 265 K. This first dehydrogenation step can be assigned to propylidyne formation. In the XPS study with Ni(100), the formation of a C₃ structure with a methyl group was observed at 200 K, and the transformation of di-σ-bonded molecular propylene into this structure was complete by 300 K. ^[8] This structure was identified as propylidyne based on DRIFTS measurements for propylene adsorption on Ni/Al₂O₃ at 298 K. ^[9] The experimental IR peaks reported for propylidyne at 1033, 1105, 1402 and 1452 cm⁻¹ for ρ (CH₃), ν (C-C), δ ₈(CH₂) and δ _a(CH₃), respectively. ^[9] are in agreement with our calculated values in Table 4.

Unlike the feature at 265 K, which is limited by H₂ desorption, the main H₂ peak at 310 K with a broad tail up to 570 K in Figure 5b is reaction limited. It demonstrates that irreversibly adsorbed hydrocarbon structures from propylidyne decomposition dehydrogenate significantly at 310 K and continue dehydrogenating up to 570 K. The absence of the v(C=C) peaks at 1416 and 1500 cm⁻¹ for hybrid di- σ/π and π -bonded propylene, correspondingly, in the IRAS spectrum at 230 K in Figure 6a confirms that these structures are no longer present at this temperature. Moreover, the calculated vibrational frequencies for propylidyne in Table 4 are also not observed at 230 K, confirming propylidyne decomposition. At 480 K, the IRAS spectrum is consistent with further dehydrogenation and decomposition: there are no longer peaks above 2800 cm⁻¹ for C-H stretches and there are fewer peaks below 2000 cm⁻¹ for other vibrations. The DRIFTS study with Ni/Al₂O₃ showed that propylidyne decomposed readily into a C₁ fragment and

ethylidyne, which in turn decomposed into another C₁ fragment and methyl.^[9] Propane decomposition on Ni to C₁ species is consistent with the TPR results in Figure 4. Only methane is detected as the gas-phase hydrocarbon product in our measurements with just a trace of propylene and without C₂ hydrocarbons. The same result was reported for a Ni/SiO₂ catalyst even when propane reacted in the presence of added H₂.^[5] In the absence of added H₂, propane decomposition necessarily produces surface carbonaceous species in addition to methane. In the XPS study with Ni(100), dehydrogenation of adsorbed propylene was complete at 370 K with the formation of carbidic carbon.^[8]

In drastic contrast with Ni, no H₂ evolution is detected in propylene TPD measurements for Ni-Sn in Figure 5b. Therefore, all chemisorbed propylene desorbs molecularly in the presence of Sn. This result is confirmed by the absence of any peaks in the IRAS spectra at 240 and 450 K in Figure 6b. Propylidyne formation and all other dehydrogenation reactions as well as cracking are completely suppressed. The DFT results explain how the Sn presence eliminates propylene decomposition and allows propylene to desorb molecularly. First, propylene is destabilized by adsorbing in the less stable π -bonded configuration on a single Ni atom due to the absence of Ni-Ni bridge surface sites and further destabilized by neighboring Sn atoms (Figure 8b), evidenced experimentally by the propylene desorption peak at a lower temperature, absence of v(C=C) for di- σ -bonded propylene and the shift of v(C=C) for the π -bonded structure to a higher wavenumber. Second, propylidyne formation on Ni-Sn becomes thermodynamically unfavorable also due to geometric and electronic effects (Figure 10c). Thus, the presence of Sn makes desorption the only pathway for adsorbed propylene both by decreasing the propylene adsorption energy and by eliminating propylidyne formation — the likely first step in cracking and additional dehydrogenation reactions.

These differences in molecular and dissociative adsorption modes provide an explanation for the higher selectivity of the Ni-Sn catalyst in propane dehydrogenation. On Ni, there are competing parallel reactions for formed propylene. It can either desorb molecularly or transform into propylidyne, which further decomposes. In contrast, formed propylene on Ni-Sn only desorbs. The additional benefit of eliminating propylene decomposition is that coke formation and, consequently, catalyst deactivation are suppressed.

Sn acts as a promoter for Ni under the tested reaction conditions because the activity of the Sn/SiO₂ catalyst with the same amount of 0.8 wt % Sn as in the Ni-Sn/SiO₂ catalyst is low. The promoting effects of Sn, which changes the catalytic properties of Ni in propane reactions by changing both the size of Ni surface ensembles and the electronic properties of Ni, are similar to the effects of Sn addition to Pt. Analogously to Ni-Sn, the presence of Sn atoms reduces the size of surface Pt ensembles, the number of neighboring Pt atoms. This leads to improvements in propylene selectivity because while propane dehydrogenation is a structure-insensitive reaction and, thus, it can proceed on a single Pt atom, cracking and further dehydrogenation side reactions are structure-sensitive, requiring multiple neighboring Pt atoms in an ensemble acting as a single catalytic site. The electronic effect was observed with X-ray absorption near edge structure (XANES) and XPS measurements that showed Pt becoming more electronegative in Pt-Sn.^[1] DFT calculations suggest that the higher selectivity of Pt-Sn can be attributed to two simultaneous effects: a lower adsorption energy for propylene and a higher activation energy for propylene dehydrogenation. [34] A lower propylene adsorption energy on Pt in the presence of Sn is evidenced by our previous TPD measurements^[35], and it is in agreement with calorimetric measurements for ethylene. [28]

The geometric and electronic effects of Sn addition to Ni for propylene are also consistent with our results for acetylene on Pt-Sn. For the geometric effects, acetylene reactions on Pt₃Sn and Pt₂Sn ordered surface alloys were compared. [19] Since the concentrations of Sn on these two surfaces are not much different, electronic promoter effects are similar. However, while there are Pt threefold sites on the Pt₃Sn surface, the arrangement of Sn atoms on the Pt₂Sn eliminates them, similarly to the elimination of Ni threefold sites on the Ni-Sn surface in the current study. The preferential mechanism for acetylene, CH-CH, transformations into vinylidene, C-CH₂, with an H transfer and into C-CH plus H with a C-H bond splitting requires a Pt-Pt bridge site for acetylene adsorption and a third neighboring Pt atom for stabilizing the reacting H atom. There is, therefore, a geometric site requirement of three adjacent Pt atoms in the form of a threefold site for these catalytic reactions. In the absence of threefold Pt sites on the Pt₂Sn surface, the reaction mechanism changes, and reactions of H transfer and C-H bond breaking become suppressed. These effects of the geometric site requirement are analogous to the elimination of the propylidyne formation on Ni-Sn.

For the electronic effects, acetylene reactions on Pt and on the same two Pt-Sn single-crystal surfaces were compared. [20] The presence of Sn destabilizes molecular acetylene on Pt sites, suppressing the formation of the strongly-bonded di- σ/π -bonded structure, which dominates on Pt. In addition, destabilization of remaining π - and di- σ -bonded acetylene structures on Pt-Sn makes thermodynamically possible a new reaction of benzene formation through trimerization in contrast with pure Pt, on which acetylene only decomposes. These electronic effects are analogous to propylene destabilization on Ni-Sn, which opens a new reaction of selective propane dehydrogenation in contrast with pure Ni, on which propylene mostly decomposes.

5. Conclusions

Propane starts reacting over the 1.5 wt % Ni/SiO₂ catalyst at 475 K by producing gasphase hydrogen and a carbonaceous residue. Above 685 K, methane becomes a major product in addition to hydrogen. Propane starts reacting over the 1.5 wt % Ni - 0.8 wt % Sn/SiO₂ catalyst (1 to 1 atomic ratio of Ni to Sn on the surface) at a higher temperature of 630 K, but the reaction products are only propylene and hydrogen. No methane or C₂ hydrocarbons are detected. Since the propane reaction activity of 0.8 wt % Sn/SiO₂ is low, Sn at this loading acts as a promoter for Ni in the Ni-Sn catalyst.

Propylene multilayer desorbs at ~100 K from both Ni(110) and c(2×2)-Sn/Ni(110) (1 to 1 atomic ratio of Ni to Sn on the surface) surfaces. The second desorption peak at 170 K for Ni is assigned to the desorption of propylene π -bonded on an atop Ni site with the characteristic v(C=C) at 1500 cm⁻¹. The desorption peak shoulder at 245 K with a broad tail extending to 265 K is assigned to the desorption of the more stable asymmetric di- σ -bonded propylene, which can also be described as a hybrid between di- σ - and π -bonded propylene. This structure adsorbs on a short bridge Ni site and has v(C=C) at 1416 cm⁻¹. The symmetric di- σ -bonded propylene is less stable, and it transforms into the hybrid di- σ/π -bonded structure on a small perturbation. Propylene structures on fourfold and long bridge Ni sites are less stable than the π -bonded structure.

On Ni-Sn, the arrangement of Sn atoms eliminates neighboring surface Ni atoms. As a result, propylene adsorbs weakly only as the π -bonded structure on an atop Ni site with $\nu(C=C)$ at 1506 cm⁻¹. This structure desorbs in a sharp single peak at 125 K. This lower desorption temperature and the higher wavenumber for $\nu(C=C)$ demonstrate that propylene is less stable on Ni-Sn than on Ni.

In addition, while propylene fully desorbs molecularly from Ni-Sn, only a fraction desorbs from Ni. Most of the adsorbed propylene on Ni decomposes. Propylene starts decomposing by forming propylidyne and surface hydrogen below 265 K. Propylidyne, in turn, decomposes, and it is not observed with IRAS at 230 K. Its decomposition produces gas-phase H₂ at 310 K. The remaining surface hydrocarbon fragments continue decomposing up to 570 K. Propylidyne adsorbs on long bridge and threefold Ni sites. The DFT calculations show that propylidyne formation becomes highly energetically unfavorable in the presence of Sn, which is confirmed experimentally by the absence of H₂ formation after propylene adsorption on Ni-Sn.

The destabilization of molecular propylene and propylidyne on Ni-Sn is due to geometric and electronic effects of Sn on Ni. The electronic effects are calculated to be more significant than the geometric. In addition, the electronic effects are calculated to be more significant for propylidyne than for propylene. The lower stability of molecularly adsorbed propylene and dissociatively adsorbed propylene as propylidyne provide an explanation for the higher catalyst selectivity of Ni-Sn in propane dehydrogenation. There are competing parallel reactions for formed propylene on Ni. Propylene can desorb molecularly or transform into propylidyne, which further decomposes. In contrast, formed propylene on Ni-Sn only desorbs, resulting in high catalyst selectivity in propane dehydrogenation. These findings will be useful in the development of improved catalysts for propane dehydrogenation to propylene and multiple other hydrocarbon reactions that require selective activation of C-H bonds without breaking C-C bonds.

Notes

The authors declare no competing financial interests.

Acknowledgements

This research was supported by the U.S. Department of Energy, Office of Science, Office of Basic Energy Sciences, under Award DE-SC0019052. The DFT calculations were performed with the Materials Studio software provided by Dassault Systèmes BIOVIA Corporation under a collaborative research agreement. We thank Dr. Felix Hanke and Dr. Victor Milman at Dassault Systèmes BIOVIA Corporation for discussions on the computational settings. We thank Dr. Tseng-Ming Chou at Stevens Institute of Technology for help with TEM measurements.

Keywords

Bimetallic, nickel, propene, spectroscopy, tin.

References

- [1] J. J. H. B. Sattler, J. Ruiz-Martinez, E. Santillan-Jimenez, B. M. Weckhuysen, *Chem. Rev.* **2014**, 114, 10613-10653.
- [2] S. Chen, X. Chang, G. Sun, T. Zhang, Y. Xu, Y. Wang, C. Pei, J. Gong, *Chem. Soc. Rev.* **2021**, 50, 3315-3354.
- [3] G. Wang, S. Zhang, X. Zhu, C. Li, H. Shan, J. Ind. Eng. Chem. 2020, 86, 1-12.
- [4] T. Wang, X. Cui, K. T. Winther, F. Abild-Pedersen, T. Bligaard, J. K. Nørskov, *ACS Catal.* **2021**, 11, 6290-6297.
- [5] Z. Yan, D. W. Goodman, Catal. Lett. 2012, 142, 517-520.
- [6] G. Wang, H. Wang, H. Zhang, Q. Zhu, C. Li, H. Shan, ChemCatChem. 2016, 8, 3137-3145.
- [7] R. Kleyna, D. Borgmann, G. Wedler, Surf. Sci. 1998, 402-404, 131-134.
- [8] C. M. Whelan, R. Neubauer, D. Borgmann, R. Denecke, H.-P. Steinrück, *J. Chem. Phys.* **2001**, 115, 8133-8140.

- [9] P. R. Marshall, G. S. McDougall, R. A. Hadden, *Top. Catal.* **1994**, 1, 9-18.
- [10] Y. D. Li, L. Q. Jiang, B. E. Koel, *Phys. Rev. B.* **1994**, 49, 2813-2820.
- [11] B. Delley, J. Chem. Phys. **1990**, 92, 508-517.
- [12] B. Delley, J. Chem. Phys. **2000**, 113, 7756-7764.
- [13] M. S. Hofman, E. V. Scoullos, J. P. Robbins, L. Ezeonu, D. V. Potapenko, X. Yang, S. G. Podkolzin, B. E. Koel, *Langmuir*. **2020**, 36, 8705-8715.
- [14] Y. Zheng, Z. Tang, S. G. Podkolzin, Chem. Eur. J. 2020, 26, 5174-5179.
- [15] E. V. Scoullos, M. S. Hofman, Y. Zheng, D. V. Potapenko, Z. Tang, S. G. Podkolzin, B. E. Koel, J. Phys. Chem. C. 2018, 122, 29180-29189.
- [16] K. Liu, T. Chen, S. He, J. P. Robbins, S. G. Podkolzin, F. Tian, *Angew. Chem., Int. Ed.* **2017**, 56, 12952-12957.
- [17] T. Chen, E. Kertalli, T. A. Nijhuis, S. G. Podkolzin, J. Catal. 2016, 341, 72-81.
- [18] T. Chen, A. Pal, J. Gao, Y. Han, H. Chen, S. Sukhishvili, H. Du, S. G. Podkolzin, *J. Phys. Chem. C.* **2015**, 119, 24475–24488.
- [19] J. Gao, H. Zhao, X. Yang, B. E. Koel, S. G. Podkolzin, Angew. Chem., Int. Ed. 2014, 53, 3641-3644.
- [20] J. Gao, H. Zhao, X. Yang, B. E. Koel, S. G. Podkolzin, ACS Catal. 2013, 3, 1149-1153.
- [21] J. Kim, L. A. Welch, A. Olivas, S. G. Podkolzin, B. E. Koel, *Langmuir*. 2010, 26, 16401-16411.
- [22] J. Kim, J. Fu, S. G. Podkolzin, B. E. Koel, J. Phys. Chem. C. 2010, 114, 17238-17247.
- [23] D. G. Barton, S. G. Podkolzin, J. Phys. Chem. B. 2005, 109, 2262-2274.
- [24] C. Xu, B. E. Koel, Surf. Sci. 1995, 327, 38-46.

- [25] L. Surnev, Z. Xu, J. T. Yates, Surf. Sci. 1988, 201, 1-13.
- [26] B. Silvi, P. Labarbe, J. P. Perchard, *Spectrochim. Acta, Part A.* **1973**, 29, 263-276.
- [27] D. R. Lide, Jr., D. Christensen, J. Chem. Phys. 1961, 35, 1374-1378.
- [28] M. A. Natal-Santiago, S. G. Podkolzin, R. D. Cortright, J. A. Dumesic, *Catal. Lett.* **1997**, 45, 155-163.
- [29] S. G. Podkolzin, R. M. Watwe, Q. Yan, J. J. de Pablo, J. A. Dumesic, *J. Phys. Chem. B.* **2001**, 105, 8550-8562.
- [30] S. G. Podkolzin, R. Alcala, J. J. De Pablo, J. A. Dumesic, *J. Phys. Chem. B.* **2002**, 106, 9604-9612.
- [31] S. G. Podkolzin, R. Alcalá, J. A. Dumesic, J. Mol. Catal. A: Chem. 2004, 218, 217-227.
- [32] Q. Zhu, G. Wang, J. Liu, L. Su, C. Li, ACS Appl. Mater. Interfaces. 2017, 9, 30711-30721.
- [33] K. Christmann, F. Chehab, V. Penka, G. Ertl, Surf. Sci. 1985, 152-153, 356-366.
- [34] M.-L. Yang, Y.-A. Zhu, X.-G. Zhou, Z.-J. Sui, D. Chen, ACS Catal. 2012, 2, 1247-1258.
- [35] Y.-L. Tsai, C. Xu, B. E. Koel, Surf. Sci. 1997, 385, 37-59.

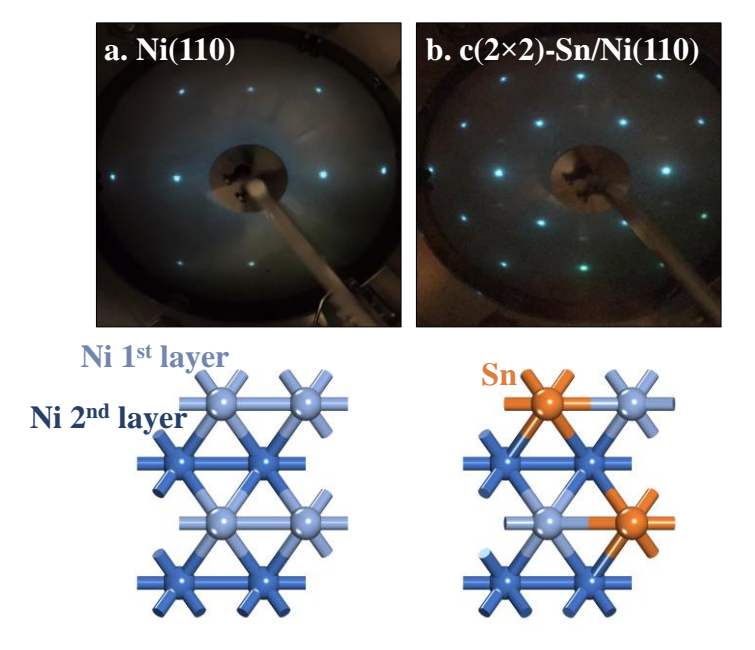


Figure 1. Top row: Low-energy electron diffraction patterns of (**a**) Ni(110) and (**b**) c(2×2)-Sn/Ni(110) surfaces at 130 eV. Bottom row: computational models of the same surfaces with only two top layers shown for clarity. The full periodic unit cells used in the density functional calculations are shown in Figure 3.

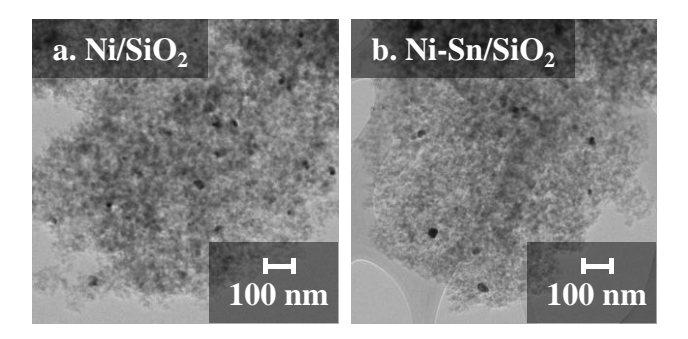


Figure 2. Transmission electron microscopy images of (a) 1.5 wt % Ni/SiO₂ and (b) 1.5 wt % Ni − 0.8 wt % Sn/SiO₂. The average Ni particle size of 20 nm was practically unaffected by the Sn deposition.

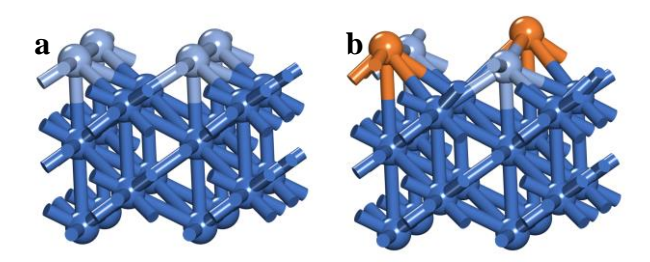


Figure 3. $2 \times 2 \times 5$ periodic unit cells used to construct infinite surfaces of (**a**) Ni(110) and (**b**) $c(2 \times 2)$ -Sn/Ni(110) for density functional theory calculations. The top views of the two top layers are shown in Figure 1.

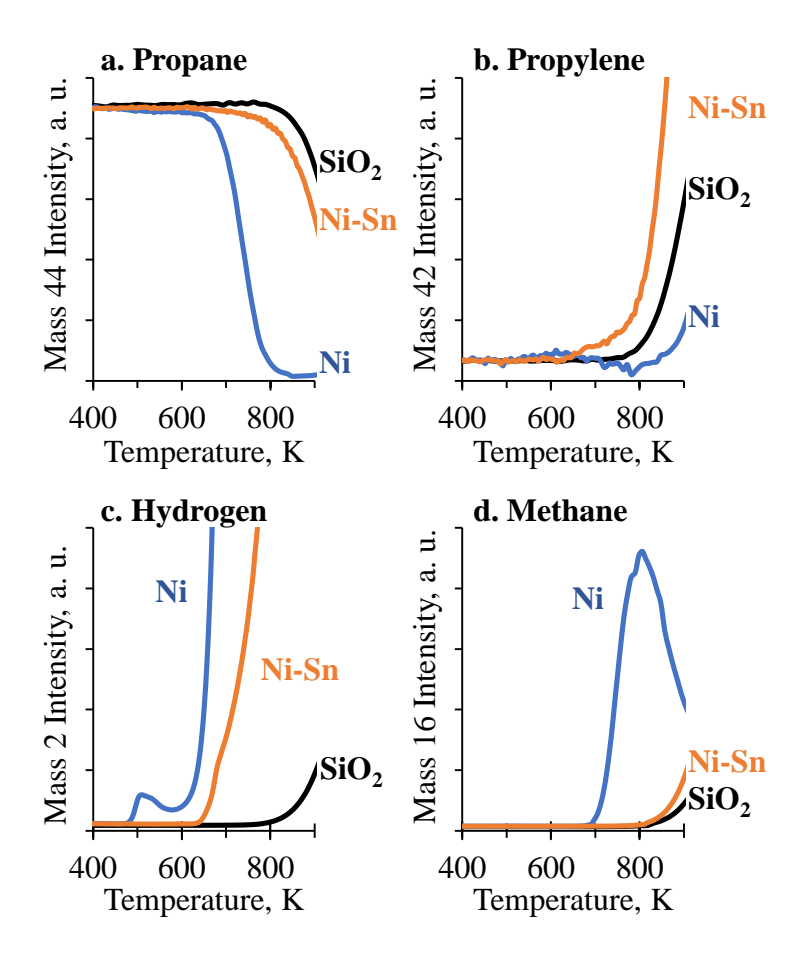


Figure 4. Mass spectra for temperature programmed reaction of propane for 1.5 wt % Ni/SiO₂, 1.5 wt % Ni – 0.8 wt % Sn/SiO₂ (1 to 1 atomic ratio of Ni to Sn on the surface) and SiO₂: (a) C₃H₈, (b) C₃H₆, (c) H₂ and (d) CH₄.

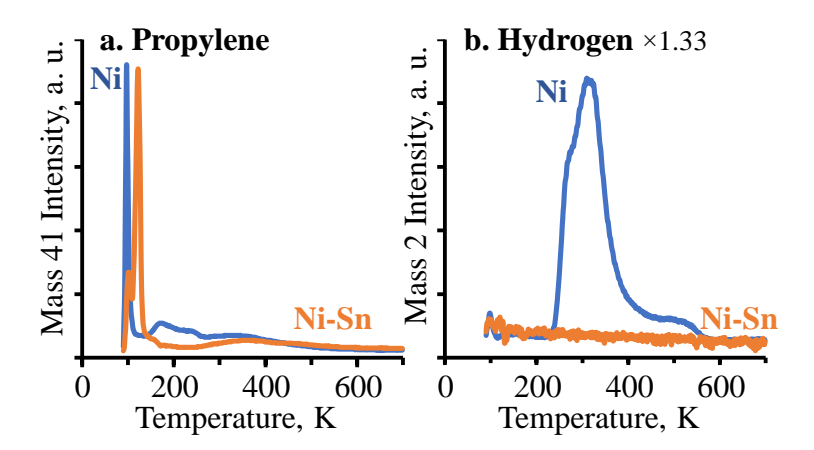


Figure 5. Mass spectra for temperature programmed desorption after propylene adsorption on Ni(110) and $c(2\times2)$ -Sn/Ni(110) surfaces: (a) C₃H₆ and (b) H₂.

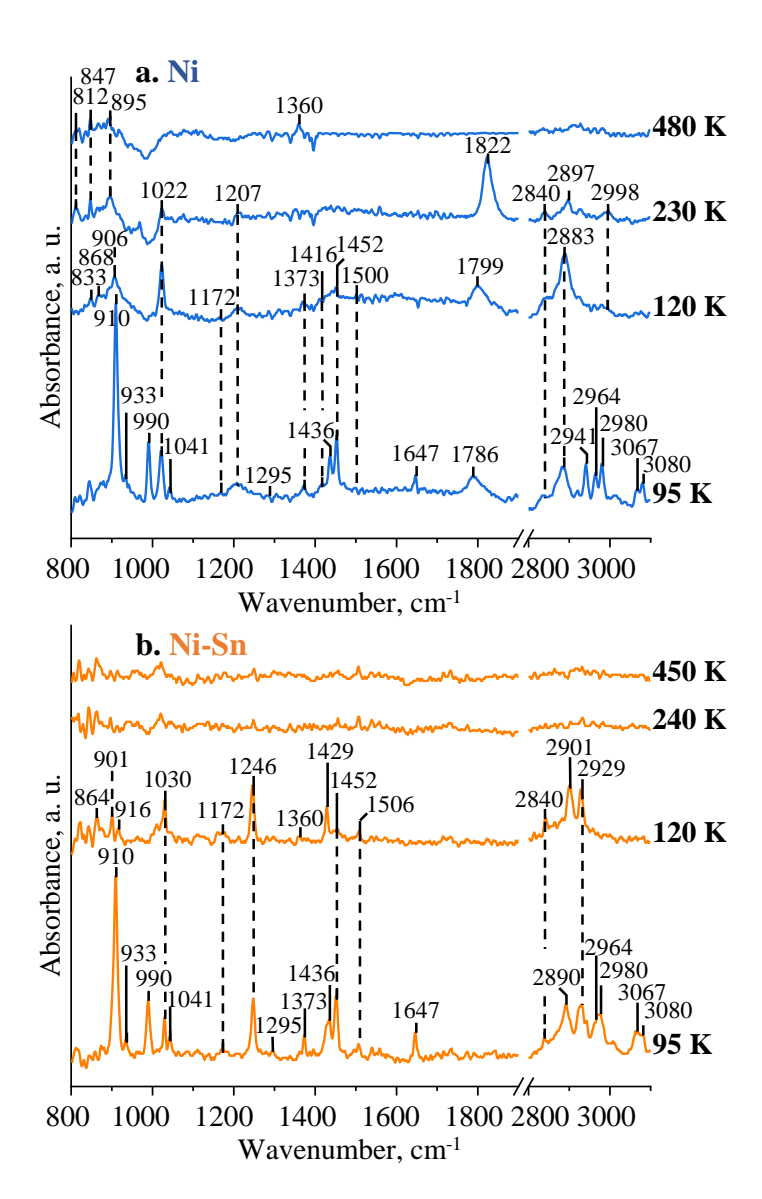


Figure 6. Infrared reflection absorption spectra as a function of annealing temperature for propylene adsorption on (a) Ni(110) and (b) c(2×2)-Sn/Ni(110) surfaces.

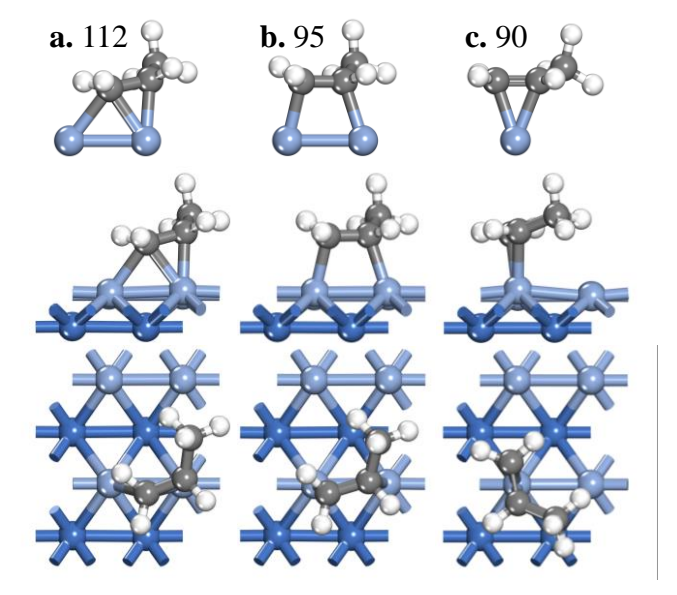


Figure 7. Structures and their adsorption energies in kJ/mol obtained with density functional theory calculations for molecular propylene on Ni(110): (a) $\mu_2\eta^2$ hybrid between di-σ- and π -bonded structures on a short bridge site, (b) $\mu_2\eta^2$ di-σ-bonded structure on a short bridge site and (c) $\mu_1\eta^2$ π -bonded structure on an atop site. Upper row: schematic with only bonding Ni atoms. Middle row: side view of the unit cell. Bottom row: top view of the unit cell. Only the top two layers of the unit cell are shown for clarity.

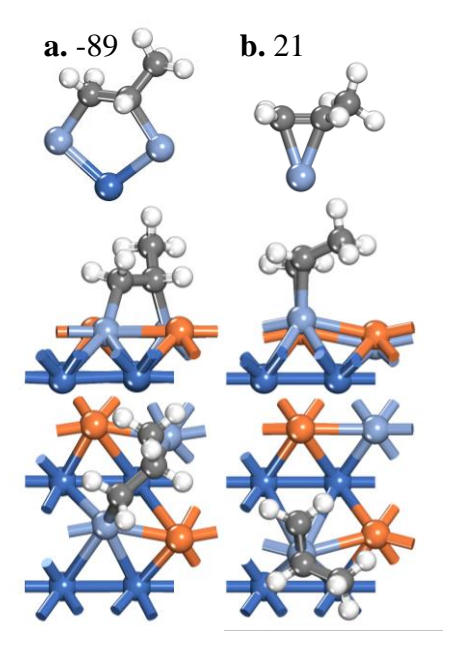


Figure 8. Structures and their adsorption energies in kJ/mol obtained with density functional theory calculations for molecular propylene on $c(2\times2)$ -Sn/Ni(110): (a) $\mu_2\eta^2$ di-σ-bonded structure on non-neighboring surface Ni atoms and (b) $\mu_1\eta^2$ π-bonded structure on an atop Ni site. Upper row: schematic with only bonding Ni atoms. Middle row: side view of the unit cell. Bottom row: top view of the unit cell. Only the top two layers of the unit cell are shown for clarity.

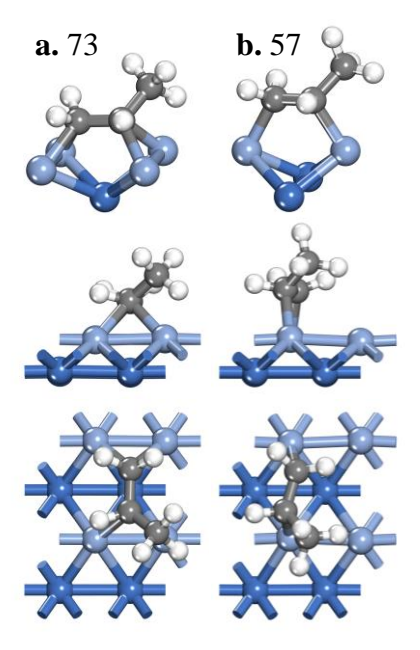


Figure 9. Less stable structures and their adsorption energies in kJ/mol obtained with density functional theory calculations for molecular propylene on Ni(110): (a) μ 4 η 2 structure on a fourfold site and (b) μ 2 η 2 di- σ -bonded structure on a long bridge site. Upper row: schematic with only bonding Ni atoms. Middle row: side view of the unit cell. Bottom row: top view of the unit cell. Only the top two layers of the unit cell are shown for clarity.

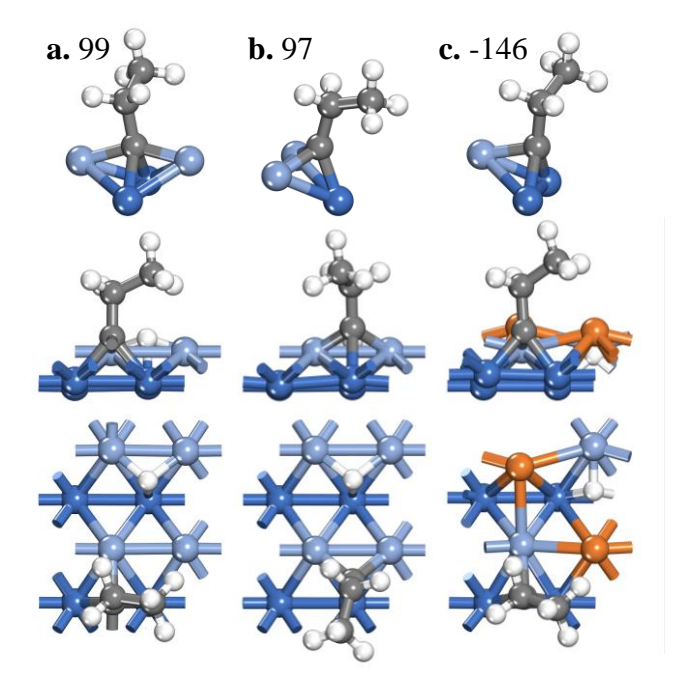


Figure 10. Structures and their adsorption energies in kJ/mol obtained with density functional theory calculations for dissociatively adsorbed propylene (propylidyne and hydrogen atom) on Ni(110): (**a**) μ4η¹ structure on a long bridge site with two additional bonding Ni atoms in the second layer, (**b**) μ3η¹ structure on a threefold site with two Ni atoms in the first layer and one Ni atom in the second layer; and on c(2×2)-Sn/Ni(110): (**c**) μ3η¹ configuration on a threefold site with one Ni atom in the first layer and two Ni atoms in the second layer. Upper row: schematic with only bonding Ni atoms. Middle row: side view of the unit cell. Bottom row: top view of the unit cell. Only the top two layers of the unit cell are shown for clarity.

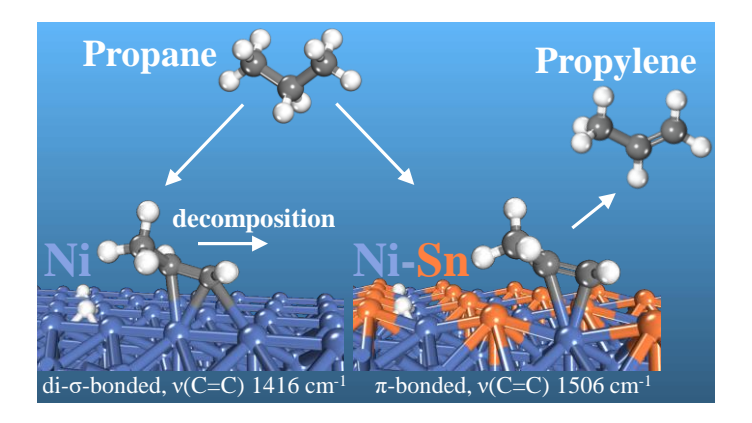


Table of Contents Graphic and Text

The reaction products of propane change significantly from mostly methane, hydrogen and surface carbon over a Ni catalyst to propylene and hydrogen over a Ni-Sn catalyst. On Ni, propylene adsorbs strongly and converts into propylidyne, which decomposes further. In contrast, propylene forms a weakly bonded structure on Ni-Sn, which desorbs fully, resulting in high reaction selectivity in propane dehydrogenation to propylene over the Ni-Sn catalyst.